Adapting the RILEM 271-ASC accelerated salt weathering test to stone/ plaster combinations: First experimental results

Lubelli, B.; Gulotta, Davide

DOI
10.1016/j.conbuildmat.2025.144435

Publication date
2025

Document Version
Final published version

Published in
Construction and Building Materials

Construction and Building Materials 502 (2025) 144435

Contents lists available at ScienceDirect

Construction and Building Materials

journal homepage: www.elsevier.com/locate/conbuildmat

Adapting the RILEM 271-ASC accelerated salt weathering test to stone/plaster combinations: First experimental results

Barbara Lubelli [a,*], Davide Gulotta [b]

[a] Faculty of Architecture and the Built Environment – Delft University of Technology, Delft, the Netherlands
[b] Getty Conservation Institute, Los Angeles, CA, USA

ARTICLE INFO

Keywords:
Render
Mortar
Salt crystallization
Accelerated weathering
SEM-EDX

ABSTRACT

Salt crystallization is one of the most common causes of decay in porous building materials. Plasters and renders, mainly due to their location at the surface of walls, where most often salt accumulation occurs, are particularly subjected to salt decay. Despite the relevance of the problem, there are no standard salt weathering tests for the assessment of the durability of plasters and renders against salt decay. This research proposes a salt weathering procedure, based on an adaptation of the RILEM TC 271-ASC recommendation, and it validates it by applying it to three plaster types (based on hydrated lime, natural hydraulic lime and hydrated lime-cement). Combined stone/plaster specimens are prepared and contaminated with 10 % (weight salt/weight solution) sodium sulphate and sodium chloride solutions. The damage development is assessed by visual and photographic monitoring, gravimetric measurements of the material loss, assessment of salt distribution in the specimens, and SEM observations supported by EDX mapping on thin sections. The results show that the test procedure is effective in causing damage in the tested plasters, within the time period of the test (about 4 months), and that damage increases with subsequent cycles. The decay severity and type differ depending on type of salt and/or of plaster. Suggestions for further improvement of the procedure are provided.

1. Introduction

Salt crystallization is a major cause of damage in porous building materials [1–3]. Despite extensive research in this field, the complexity of the problem has hindered until now the use of numerical models for forecasting decay due to salt crystallization [4,5]. Nowadays, in the practice of construction and conservation, the durability of porous building materials with respect to salt crystallization, when not well-known from past field experience, is mostly determined by accelerated ageing tests [6–8]. Recently, a new test procedure has been developed by the RILEM Technical Committee TC 271-ASC and validated by round robin tests and field observations [9,10]. This procedure reproduces the mechanism of salt damage triggered by capillary transport of salt solution towards the evaporation surface of a material, as it can happen in the case of rising damp in walls. The procedure proposes a new approach [7], different from other salt crystallization tests, and derived from a common approach to the durability of reinforced concrete [11]. It starts from the consideration that a critical degree of salt accumulation, i.e., degree of pore filling [12], is needed to initiate the damage. Salt damage is thus seen as a process developing in two stages: salt accumulation followed by damage propagation. The procedure aims to replicate this process: in the accumulation stage salts are introduced into the material and accumulated at the evaporation front (generally near the surface) during drying; in the propagation stage, salt dissolution and recrystallization cycles are induced by re-wetting with liquid water followed by drying and/or by changes in air RH to stimulate the occurrence of damage.

The RILEM TC 271-ASC procedure proved successful in reproducing salt decay in a reliable way in different brick and stone types, tested as single materials. However, the procedure is not directly suitable for assessing the durability of mortars. Past research has unequivocally demonstrated that the behaviour of mortar is strongly affected by the moisture transport properties of the substrate/mortar system [13]. This has been further investigated for mortars used as plasters[1] [14,15], showing that accelerated aging procedures assessing the durability of plaster as a single material [16] might thus provide unreliable results. Therefore, the aim of this work is to propose a new, accelerated procedure for assessing the resistance of plasters to salt crystallization

* Corresponding author.
E-mail addresses: b.lubelli@tudelft.nl (B. Lubelli), dgulotta@getty.edu (D. Gulotta).

[1] In this paper, for the sake of simplicity, only the term plaster is used to refer to both interior and exterior application.

https://doi.org/10.1016/j.conbuildmat.2025.144435
Received 8 August 2025; Received in revised form 4 November 2025; Accepted 5 November 2025
Available online 12 November 2025

Table 1
Composition, water content and flow of the fresh plasters.

Acronym	Binder	binder/ aggregate ratio (by vol.)	Water content (% of dry mass)	Flow (mm)
AL	Air lime	1:2	18	160
NHL	Natural hydraulic lime	1:3	14	165
AC	Air lime and Portland cement	1:3 (4:1:15)	14	160

Table 2
Types of specimens, shape and size, and tests.

	Materials	Shape and size	Tests
Type A	Mortar	Prisms; 40 × 40 × 160 mm	Compressive strength
Type B	Mortar	Discs; 50 mm diameter, 20 mm height	Water absorption by capillarity; porosity by immersion; drying behaviour; MIP
Type C	Combined mortar and stone system	Cylinders: 50 mm diameter, 30 mm thick substate + 20 mm thick plaster layer	Optical microscopy on thin section; salt weathering test

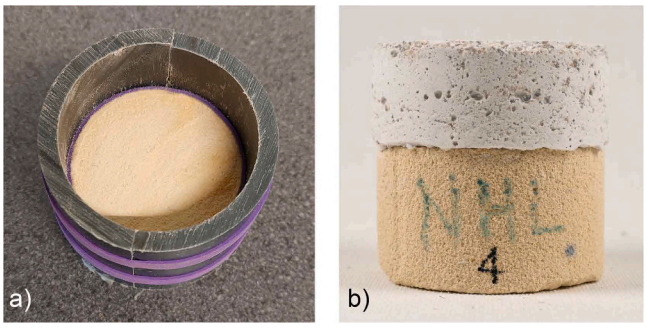

Fig. 1. Stone substrate encased inside the mould before application of the plaster layer (a), and a complete specimen type C (stone+plaster) after removal of the mould and curing (b).

damage in an effective and reliable way. To this scope, the RILEM TC 271-ASC procedure has been adapted to be applied on combined substrate/plaster specimens. The effectiveness and reliability of the procedure have been assessed by testing the durability of three different plaster types used in combination with limestone as a substrate. Knowledge developed in previous research [17–19] has contributed to the definition of procedure, as detailed in the next sections.

2. Materials and methods

2.1. Materials

Three types of plasters were selected for the test:

- Air lime plaster (AL), prepared by mixing air lime (Supercalco 90 by Carmeuse, bulk density 580 kg/m^3) with sand in proportion 1:2 by volume;
- Natural hydraulic lime plaster (NHL); prepared by mixing moderately hydraulic lime (type 3.5 by Saint Astier, bulk density 700 kg/m^3) with sand in proportion 1:3 by volume
- Air lime and Portland cement (CEMI 42.5 by ENCI, bulk density 1310 kg/m^3) plaster (AC), prepared by mixing the binders and the sand in 4:1:15 by volume.

In all plasters, quartz sand with a standard grain size distribution between 0.08 and 2 mm (CEN Standard sand according to EN 196–1 [20], bulk density 1700 kg/m^3) was used. The water content and the workability of the fresh plasters, measured according to EN 1015–3 [21], are reported in Table 1.

The plasters were applied on a Maastricht limestone substrate (see Section 2.2). Maastricht limestone is a soft (compressive strength between 3 and 5 MPa), yellow colored limestone constituted up to 94–98 wt% by calcium carbonate. It has a very high open porosity (about 50 %) with a unimodal pore size distribution (pore diameter 35–40 μm) [22].

2.2. Specimen preparation

For each plaster type, specimens of different sizes were prepared to be used in the different characterization and weathering tests (Table 2).

The size of type C specimens is defined by making reference to the specimens used in the salt weathering test developed by the RILEM TC 271-ASC, which suggests using cylinders of 50 mm diameter and 50 mm height. This small specimen size allows for fast absorption and drying in comparison to other procedures testing combinations of materials [23]. Maastricht stone has been chosen as substrate because of its high and coarse porosity; these characteristics allow for a large salt solution reservoir, and favour fast salt solution transport by capillarity towards the plaster. Overall, these properties promote rapid absorption and drying, and combined with the small specimen size, contribute to speeding up the weathering test.

Specimens type A were prepared in polystyrene moulds. Specimens type B and C were prepared on top of the limestone substrate (Fig. 1). Specimens type B were detached from the substrate after 3 days of curing; a paper tissue was interposed between the substrate and the fresh plaster during preparation, to facilitate detachment of the plaster layer. Specimens type B were prepared on a porous substrate, as it is known that the porosity and pore size of mortars are affected by the suction of the substrate [24,25], and thus mortars produced in non-absorbing moulds might not be fully representative of actual application conditions. The limestone cylinders were wetted prior to the application of the plaster, to avoid excessive suction of water from the fresh mortar; in the case of the air lime plaster, a lime slurry was applied with a brush to the surface of the stone in order to increase the adhesion.

All specimens were cured for a week at 95 % ±5 % RH and then stored at 65 % ±5 % RH for at least 21 days (according to EN 1015–11 [26]) and until the moment of testing.

2.3. Characterization tests

Different characterization tests were performed to determine the properties of the hardened plaster. The compressive strength of the plasters was assessed in threefold on specimens type A, according to EN1015–11 [26], at both 28 days and 90 days from casting.

The water absorption by capillarity was measured in threefold on plaster discs (specimens type B). The plaster specimens were dried at 40°C in an oven until constant weight and then sealed on their lateral surface with parafilm tape. Water was poured into a container on the bottom of which a plastic grid had been placed; care was taken to keep the water level at about 2 mm above the grid surface and to maintain the water level constant during the execution of the test. The specimens were placed with their bottom surface (originally in contact with the stone substrate) on the grid and their change in weight was recorded at regular intervals. Based on the results, the water absorption curves were drawn and the capillary water absorption coefficient (WAC) was calculated as the slope of the initial, linear part of the absorption curve.

Density and drying behaviour were tested on the same specimens after they reached saturation. Specimens were submerged in water for 24 h. Afterwards, the weight of the saturated specimens in air (Mw_{air}) and under water (Mw_{water}) was recorded and the density D [kg/m^3] and porosity P [vol%] were calculated as follows:

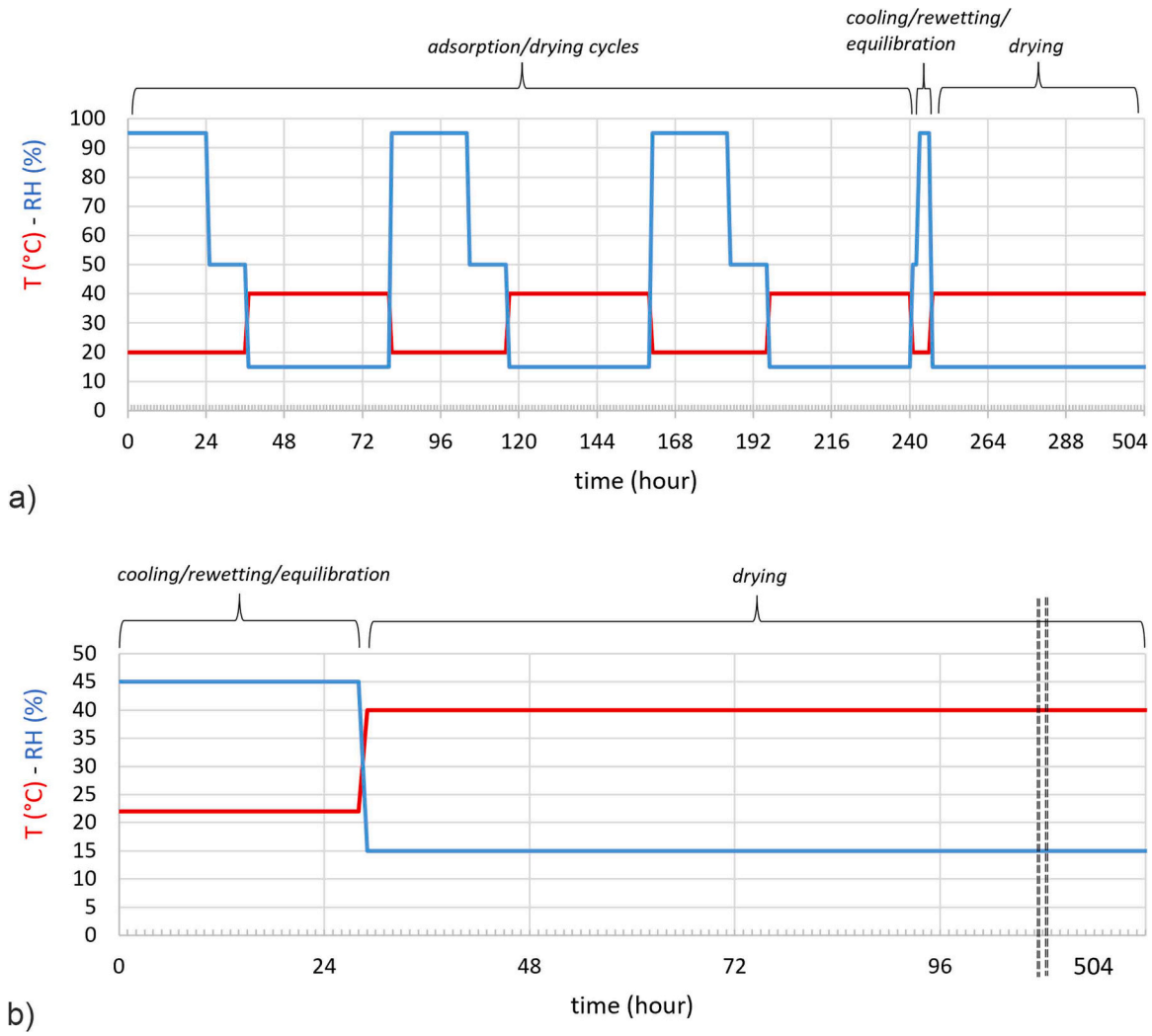

Fig. 2. Three-week temperature and RH cycle of the propagation stage for specimens contaminated with NaCl (a) and Na_2SO_4 (b).

$$D = Md/(Mw_{air} - Mw_{water})$$

$$P = 100*(1-D/2650)$$

where 2650 kg/m^3 is a reference density value for a stone-like building material with no pores [27].

The bottom surface of the specimens was then sealed and the specimens were set to dry at room conditions (Temperature = 22 ± 2 °C; Relative Humidity = 45 ± 5 %). The weight of the plaster was recorded at regular intervals during drying.

The open porosity and the pore size distribution of the plaster were determined by Mercury Intrusion Porosimeter (MIP) (Autopore IV 9500 by Micromeritics) on two samples of about 1 cm^3 for each of the plaster types. Samples for MIP analyses were collected from the core of type B specimens.

The pore structure of the plasters was further investigated using a VHX-6000 digital microscope (KEYENCE, Itasca, IL, USA) with a 1/1.8-inch CMOS image sensor (1600 × 1200 pixels resolution) on thin sections (one for each plaster type) prepared from specimen type C, including the plaster layer on top of the limestone substrate. Thin sections had 30 μm thickness, and were impregnated with yellow, fluorescent resin. Overview and detailed pictures of the plaster and its interface with the stone were collected at different magnifications.

Thin sections of the samples at the end of the weathering test were prepared by embedding them in epoxy resin. Water-free polishing was used during preparation to avoid alterations in the salt distribution. Thin sections were carbon-coated prior to the SEM-EDX analysis, conducted with a ZEISS GeminiSEM 300 microscope, equipped with an Oxford X-Max detector for elemental mapping, working in variable pressure conditions with a back-scattered detector and 10.00 kV energy.

2.4. Salt weathering test

2.4.1. Procedure

Specimens type C were subjected to a salt weathering test in the laboratory. The test procedure used is based on the RILEM TC 271-ASC procedure [9], adapted to make it suitable for testing plasters.

In the accumulation stage, the specimens were contaminated with 10 % (salt weight/solution weight) solutions of Na_2SO_4 and NaCl (Sigma Aldrich, ACS reagent grade). The two salts were tested separately, as single salts. The amount of the salt solution to be introduced in the specimen was calculated to equal the capillary moisture content (CMC),

Table 3
Compressive strength measured at 28 and 90 days.

	Compressive strength (MPa)	
	28 days	90 days
AL	0.53 *(±0.09)*	1.74 *(±0.06)*
NHL	0.53 *(± 0.04)*	0.77 *(±0.06)*
AC	1.21 *(± 0.06)*	1.38 *(±0.03)*

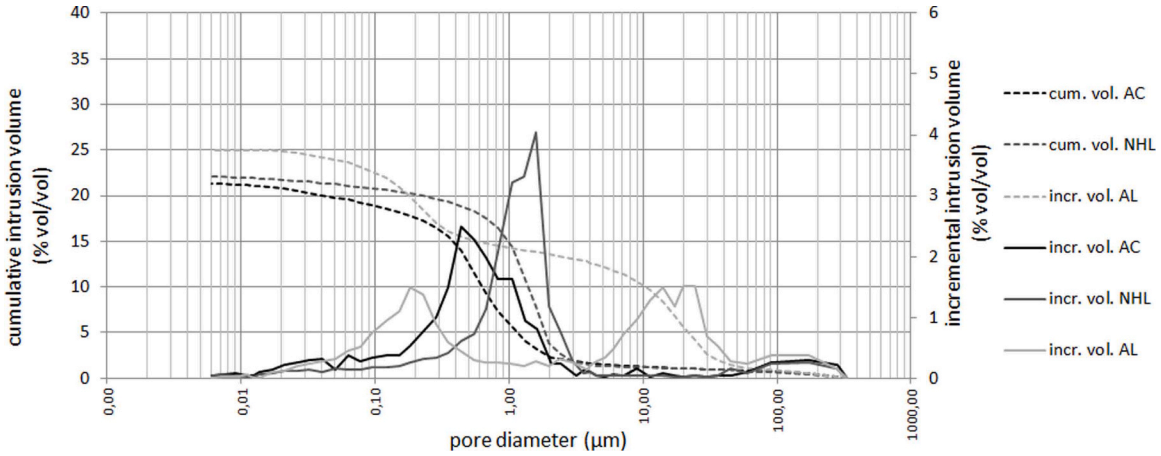

Fig. 3. Open porosity (cumulative intrusion volume) and pore size distribution (incremental intrusion pore volume) of the different plasters as determined by means of MIP. For readability reasons, only one of the two measurements is reported for each plaster type.

Table 4
Porosity as assessed by MIP and immersion at atmospheric pressure.

Plaster	Porosity as measured by MIP (vol%)	Porosity as measured by immersion at atmospheric pressure (vol%)
AL	24.54 *(±0.49)*	29.28 *(±0.34)*
NHL	21.07 *(±1.04)*	25.53 *(±0.52)*
AC	21.92 *(±0.59)*	25.97 *(±0.11)*

i.e., the water content at the end of the first stage of water absorption by capillarity (see [9] for details) of the stone substrate. This choice is preferred to the option of complete saturation of the specimens with salt solution, as it allows to compare plasters with different absorption behaviours (including plaster with water repellent additives mixed in the mass) in comparable conditions, and to assess the easiness by which salt solution migrates from the substrate into the plaster [28,29]. The CMC was determined by performing a water absorption test by capillarity, according to the same procedure described in Section 2.3, on 3 stone cylinders of 50 mm diameter and 30 mm height; the average CMC was then used for defining the amount of solution to be introduced in the specimens. After contamination, the specimens were dried at 40°C 15 % RH until at least 80 % of the water was evaporated.

At this point, the damage propagation stage started; as in the RILEM TC 271-ASC procedure, this stage differs between Na_2SO_4 and NaCl contaminated specimens, to optimize the effectiveness of the test. In the case of Na_2SO_4, each 3-week cycle includes rewetting with liquid water and drying (Fig. 2b), to favour dissolution of thenardite and crystallization of mirabilite at high supersaturation [30,31]. In the case of NaCl, each 3-week cycle starts with rewetting with liquid water by capillary absorption from the bottom of the specimen, followed by temperature (20–40°C) and RH (15–95 % RH) cycles to induce hygroscopic moisture uptake/release and thus repeated dissolution and recrystallization cycle of the salt (Fig. 2a), known to be particularly effective in causing damage [32,33] (please refer to [9,34,35] for further details). In both cases, the propagation stage consisted of 4 cycles.

2.4.2. Assessment of damage and salt distribution

At the end of the propagation stage, the specimens were brushed, and the debris was separated from the salt present in the debris by filtration, following the procedure described in [9]. The amount of material loss and salt efflorescence was determined gravimetrically.

Additionally, the salt distribution was assessed at the end of the accumulation and propagation stages in a subset of specimens. The specimens were ground up to the following depths from the evaporation surface: 0–2 mm, 2–5 mm, 5–10 mm, 10–20 mm, 20–30 mm, 30–40 mm, 40–50 mm. The debris and/or salt efflorescences present on the surface of the specimens were brushed and collected, before grinding the specimens. The salt distribution at different depths was assessed by

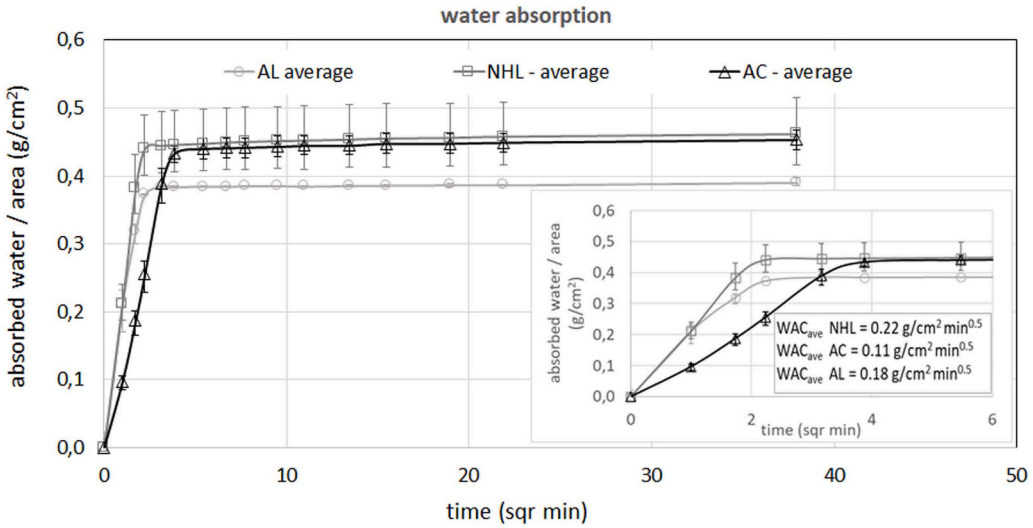

Fig. 4. Water absorption curve of the plasters (average of 3 specimens and standard deviation); the insert shows the early-stage absorption and the WAC.

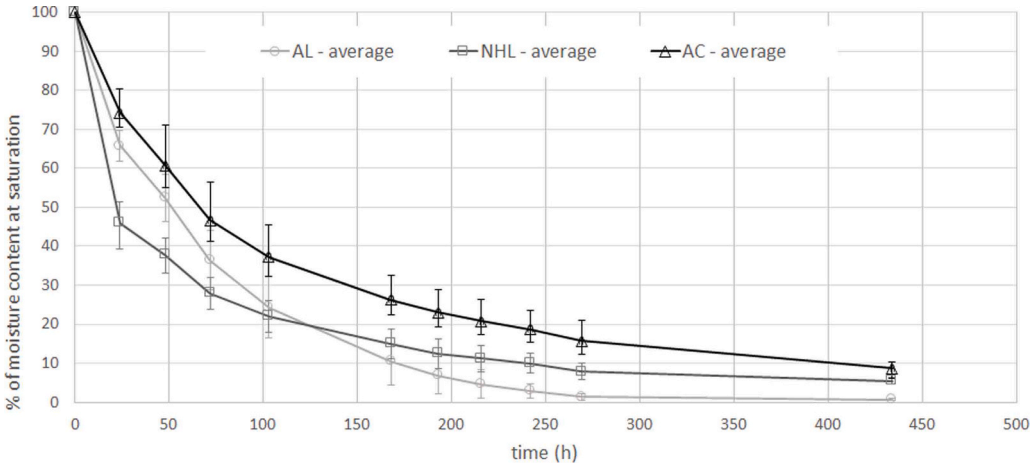

Fig. 5. Drying curves of the plasters (average of 3 specimens and standard deviation).

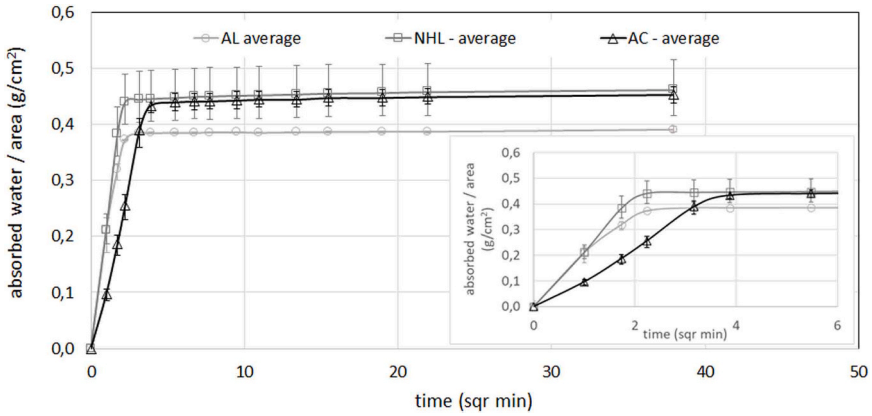

Fig. 6. Digital microscopy images of AL, NHL and AC plasters. Overview pictures (left) and detail (right) of the plasters' microstructural features.

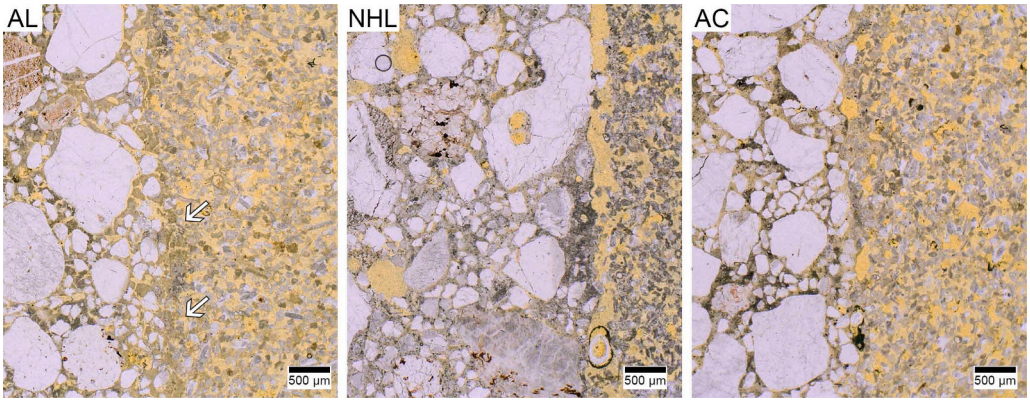

Fig. 7. Detail of the plaster/limestone interface; digital microscopy images of AL, NHL and AC (transmitted light).

measuring the hygroscopic moisture uptake (HMC) of the powder samples after storing them at 20 °C, 95 % RH for 30 days. The HMC gives an indication of the presence of hygroscopic salts and, in the case of contamination with a single salt, as in this case, it can be reliably related to the salt content [36–39].

The hygroscopic moisture content (HMC) of the samples was calculated as follows:

HMC = 100 *(sample weight at 95% RH – sample dry weight) / sample dry weight

The dry weight was measured immediately after cooling down of the samples at room conditions (temperature 22 ± 2°C, 45 ± 5 % RH). Additionally, at the end of the propagation stage, one thin section for each plaster and salt type combination was prepared, and observed by means of Scanning Electron Microscopy-EDX analysis (ZEISS Gemini SEM 300, Jena Germany). In order to avoid dissolution of the salts, thin sections were prepared without the use of water; sections were left uncovered to allow for EDX analysis.

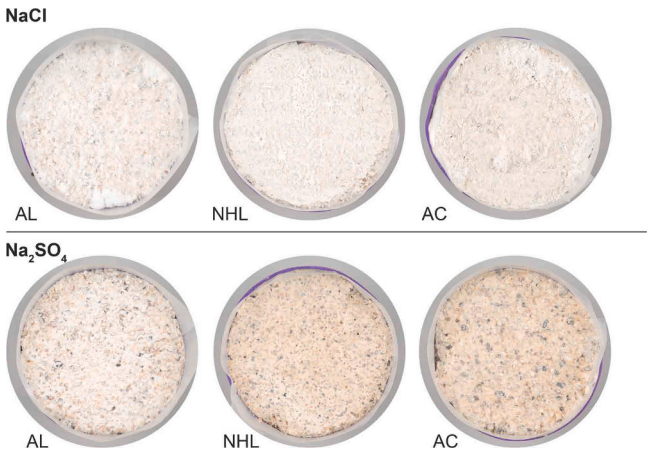

Fig. 8. NaCl - and Na_2SO_4-contaminated specimens at the end of the accumulation stage.

3. Results

3.1. Characterization tests on plaster

3.1.1. Mechanical strength

The results of the compressive strength of the plasters at 28 and 90 days are reported in Table 3. NHL plaster has a very low compressive strength at 28 days, which does not significantly increase with curing time, i.e., after 90 days. The NHL plaster has the lowest compressive strength among the tested plasters. AC plaster shows the highest strength at 28 days, which, however, does not significantly increase with time. After 90 days of curing, AL plaster has the highest compressive strength. The low mechanical strength measured in NHL and AC plaster might be due to the curing conditions (1 week at 95 % RH followed by 3 weeks at 65 % RH, as prescribed by [26]), not allowing for sufficient hydration and thus strength gain.

3.1.2. Open porosity and pore size distribution (MIP)

The open porosity and pore size distribution of the plasters, as measured by MIP, are reported in Fig. 3 and Table 4. All plasters have quite comparable open porosity. AL plaster has the highest open porosity (24.54 ± 0.49 vol%), whereas AC and NHL plasters show similar, lower porosity values (21.92 ± 0.59 vol% and 21.07 ± 1.04 vol % respectively).

The pore size distribution of the AL plaster is clearly bimodal, with two groups of pores, one in the 0.05–0.5 micrometre range, and another in the 5–30 micrometre range. Differently, plasters AC and NHL show pores within a single size range, 0.3–2 micrometre and 0.5–3 micrometre, respectively. Pores and voids larger than 400 μm, present in all the studied plasters and detected by digital microscopy, cannot be measured by MIP.

3.1.3. Water absorption and drying

The capillary water absorption behaviour at atmospheric pressure of the plasters is shown in Fig. 4.

The porosity of the plasters, as measured by immersion at

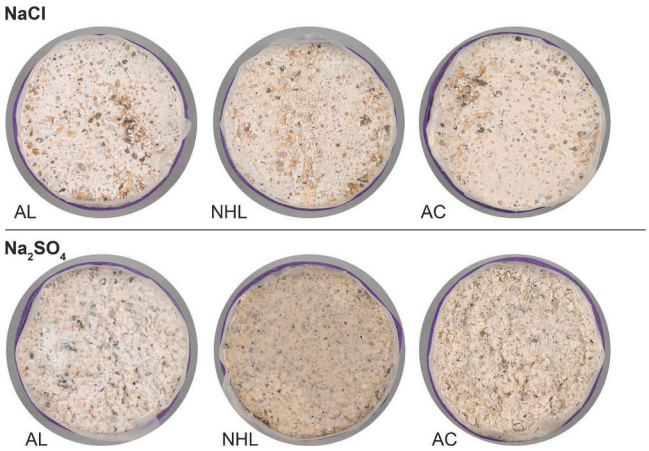

Fig. 10. NaCl- and Na_2SO_4-contaminated specimens at the end of the propagation stage.

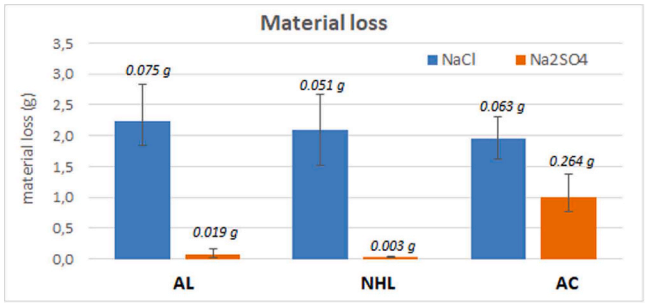

Fig. 11. Material loss at the end of the test (average of 3 specimens); the numbers in italics refer to the amount of salt in the debris.

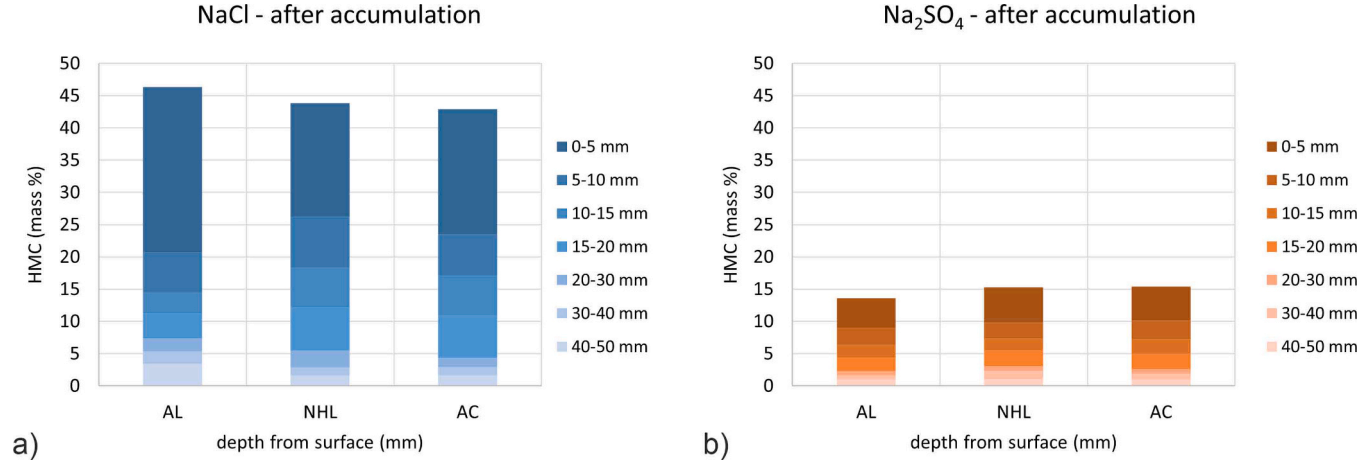

Fig. 9. HMC distribution in NaCl (a) and Na_2SO_4 (b) contaminated specimens at the end of the accumulation stage (data from one specimen for each plaster/salt combination).

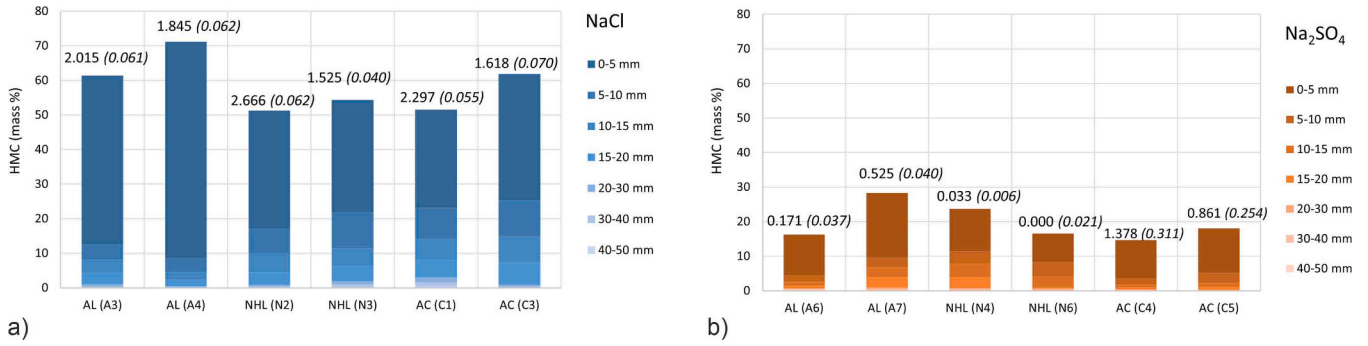

Fig. 12. HMC distribution in NaCl- (a) and Na_2SO_4-contaminated specimens (b) at the end of the test (2 specimen for each plaster/salt combination). The number above the bars reports the material loss, and the amount of salts in the debris (between brackets and in italics).

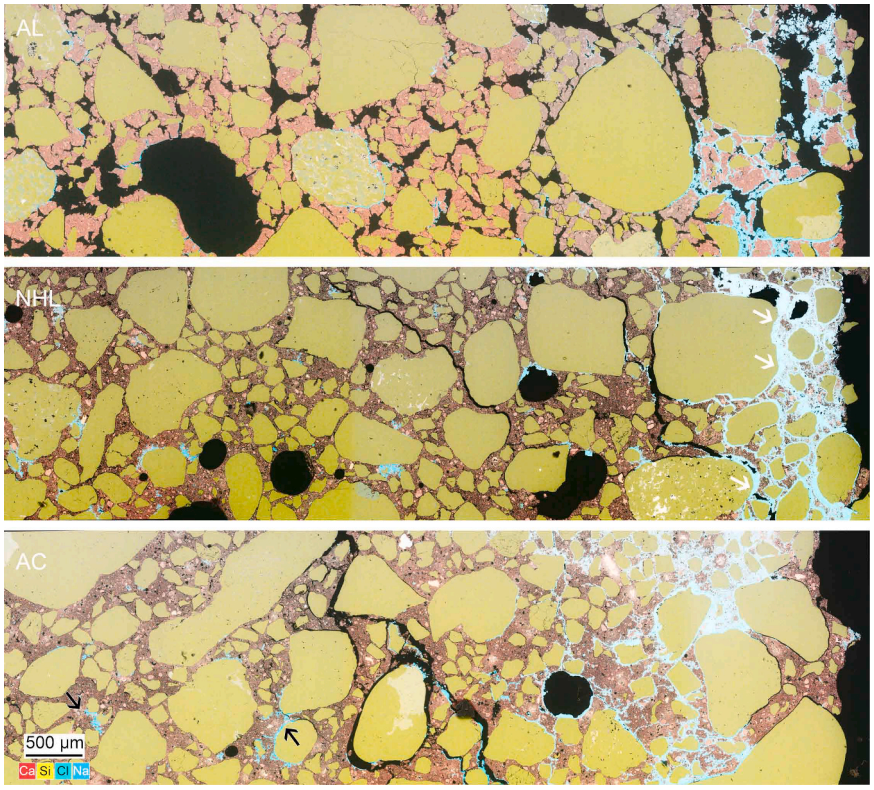

Fig. 13. EDX maps of the section of AL, NHL and AC plaster specimens, contaminated with NaCl, at the end of the test; the evaporation surface is on the right.

atmospheric pressure, varies between 26 vol% for AC and NHL, and 29 vol% for AL plaster. It can be observed that these porosity values are higher than those measured by MIP (Table 4). This difference can be due to the presence of voids larger than 400 µm, which cannot be measured by MIP. However, the relative differences between the plasters are similar: also in this case, NHL and AC plasters show a similar porosity, lower than that of AL plaster.

The water absorption coefficient, i.e. the slope of the initial, linear part of the curve, shows that AC plaster has the slower absorption rate; NHL plaster shows the fastest absorption rate, slightly higher than that of AL plaster.

Fig. 5 reports the drying behaviour of the plasters. Similarly to what observed in the water absorption test, NHL plaster shows the fastest drying, followed by AL and AC plasters. After about 3 weeks, NHL plaster is fully dry, whereas AL and AC plasters still retain 5–10 % of the initial moisture content. The fast absorption and drying of NHL plaster can be related to the large amount of pores in the capillary range (see Fig. 3).

3.1.4. *Plaster characterization by digital microscopy*

Thin section micrographs of the specimens are shown in Fig. 6. These images clearly show the differences between the structure and porosity of the investigated plasters. NHL plaster looks very lean, with a large amount of voids; an uneven distribution of the binder is observed (Fig. 6-NHL). AC plaster, despite having the same 1:3 binder/aggregate ratio as NHL plaster, looks more compact, with some large voids, both round (air bubbles) and irregularly shaped (compaction voids) (Fig. 6-AC). The AL plaster looks more compact than the NHL plaster, as expected because of its 1:2 b/a ratio; the visible porosity is constituted mainly by shrinkage cracks in the binder, and large voids (max diameter about 1 mm) (Fig. 6-AL). It can be supposed that these cracks contribute to the 5–30 µm pore interval measured by MIP.

When looking at the interface between the plaster and the stone substrate (Fig. 7), it can be seen that voids are present at this interface in the NHL specimen, indicating areas of locally low adhesion. Differently, the AC and AL plaster shows a good adhesion to the limestone substrate. In the case of the AL specimen, the lime slurry applied onto the stone

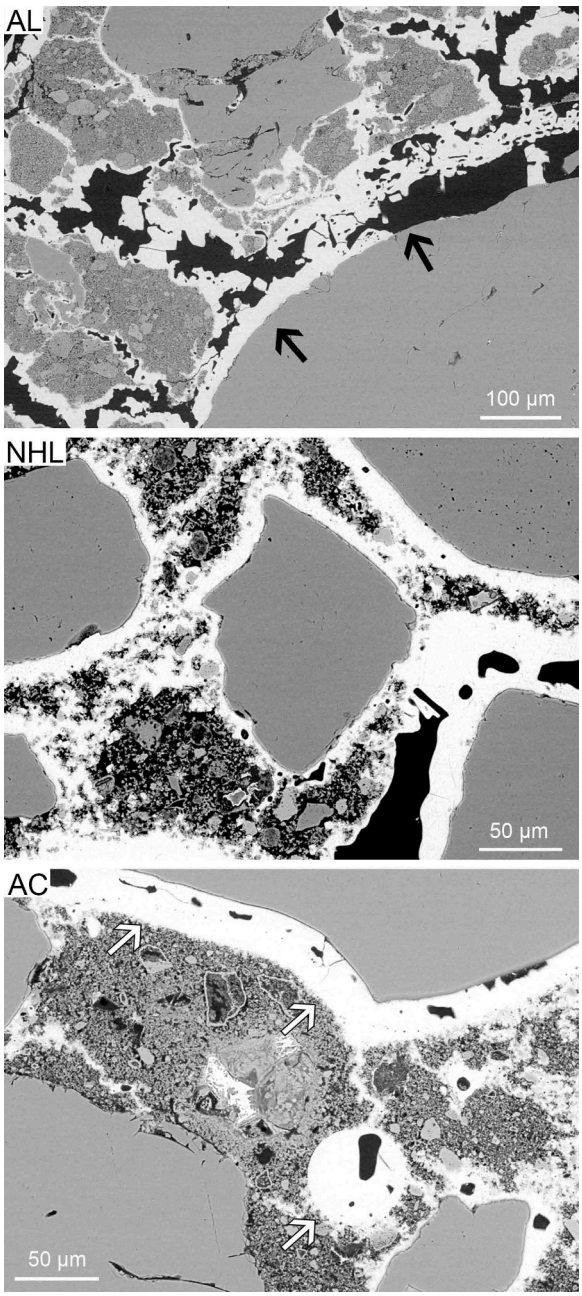

Fig. 14. SEM (Back Scattered Detector mode) images of AL, NHL and AC plasters contaminated with NaCl at the end of the test: details of the evaporation surface after brushing.

before the plaster is visible as a lime-rich layer at the interface (Fig. 7, white arrows).

3.2. Weathering test

3.2.1. Accumulation stage

Fig. 8 shows the surface conditions of representative specimens, contaminated with NaCl and Na_2SO_4, at the end of the salt accumulation stage. At this point, none of the specimens showed damage; this is consistent with the requirements for this procedure, which aims at separating the initial salt accumulation process from damage initiation and propagation. In most NaCl-contaminated specimens, efflorescences were visible on the surface; these were more evident on AL plaster than on NHL and AC plasters. Differently, none of the Na_2SO_4-contaminated specimens showed efflorescences. This behaviour confirms the higher tendency of sodium chloride to crystallize at the surface in comparison to sodium sulphate [40–42].

The HMC distribution at the end of the accumulation stage is reported in Fig. 9. The HMC values in sodium chloride-contaminated specimens are higher than those measured in Na_2SO_4-contaminated specimens, due to the higher hygroscopic moisture uptake of this salt in comparison to sodium sulphate [43]; comparisons of HMC values can thus only be done among samples contaminated with the same salt. NaCl-contaminated specimens show a higher relative percentage of salts accumulated in the outer layer (0–5 mm) (40–55 % of the total amount of salt left in the specimen), in comparison to Na_2SO_4-contaminated specimens (33–36 %). This confirms once again the tendency of sodium chloride to be more easily transported towards the evaporation surface than sodium sulphate.

3.2.2. Propagation stage

3.2.2.1. Evolution of the damage. Fig. 10 shows the surface conditions of representative specimens at the end of the propagation stage, i.e., at the end of the test.

In NaCl-contaminated specimens, damage was first observed in AL and NHL specimens, in the form of scaling of the superficial binder-rich layer, after the first cycle of the propagation stage. In the following cycles, in addition to scaling, sanding also developed and damage increased with time. AC specimens suffered damage, in the form of sanding, starting from the end of the 2nd cycle; also in this case, damage increased with time. The amount of efflorescence on the surface of NaCl-contaminated specimens during the propagation stage was limited, and much less than observed at the end of the accumulation stage.

In Na_2SO_4-contaminated specimens, damage became visible only during the 4th cycle of the propagation stage in AL plaster, in the form of minor sanding, and in AC plaster as moderate crumbling and scaling. NHL specimens did not show any granular disintegration of the surface, but a noticeable colour alteration, seen as dark patina, developed over the surface already after the first cycle. No significant amount of efflorescences was observed on Na_2SO_4-contaminated specimens, with the exception of AC-specimens at the end of the test.

3.2.2.2. Gravimetric assessment of material loss and efflorescence. The material loss and amount of salt present in the debris at the end of the test are reported in Fig. 11. In general, the NaCl-contaminated specimens show a higher material loss than Na_2SO_4 contaminated specimens, confirming the results from the photographic monitoring of the damage during the test.

The material loss in the NaCl-contaminated specimen is moderate (about 2 g), and the differences among different plaster types are minor. The amount of salts present in the debris is low, corresponding to less than 3.2 % of the salt originally introduced in the specimens. This suggests that most of the salt is still concentrated within the outer layer of the specimens.

Among Na_2SO_4-contaminated specimens, only the AC plaster showed some material loss; no significant material loss was recorded in the case of AL and NHL plaster. The higher material loss among all the Na_2SO_4-contaminated specimens is associated with the larger amount of salt in the collected debris.

3.2.2.3. Salt distribution in depth. Fig. 12 shows the salt distribution in the specimens (two for each plaster/salt combination) at the end of the propagation stage, after brushing of the debris from the surface. Similarly to what observed at the end of the accumulation stage, the HMC distribution is similar in all specimens, independently of plaster and salt types: salts accumulate in the plaster layer, confirming the good moisture transport properties of these plasters.

In the case of NaCl-contaminated specimens, AL plaster shows a slightly higher accumulation of salt (up to 88 % of the salt amount left in

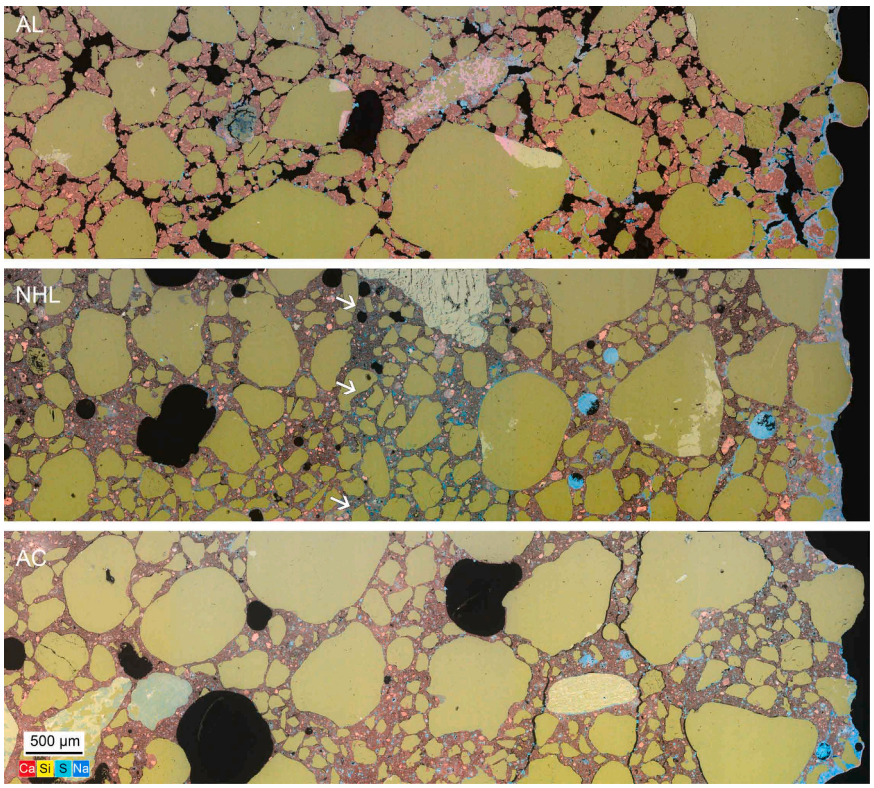

Fig. 15. EDX maps of the section of AL, NHL and AC plaster specimens, contaminated with Na_2SO_4, at the end of the test; the evaporation surface is on the right.

the specimen) in the outer layer of the plaster (0–5 mm) than NHL (up to 67 %) and AC (up to 59 %) plasters. This shows that the AL plaster has the most efficient moisture and salt transport behaviour. Differently, in the case of Na_2SO_4, a higher percentage of salt was accumulated in the outer layer of the AC plaster, compared to AL and NHL plasters: this is in agreement with the final conditions of AC specimens showing damage at the end of the test.

When comparing the HMC distribution after the accumulation stage and at the end of the test, it can be concluded that further accumulation of salts towards the surface (decrease of HMC in stone, and increase of HMC in outer plaster layer) has occurred. This indicates that the additional wetting/drying cycles have effectively promoted salt migration and accumulation towards the evaporation surface, and also confirms that the duration of the wetting/drying periods during the propagation stage avoids salt redistribution in-depth.

3.2.2.4. Microscopy observations of damage and salt distribution. SEM observations and EDX analyses have been performed to investigate the salt distribution according to the specimens' depth and any salt crystallization-induced microstructural damage, complementing the HMC results with higher resolution and providing spatially-resolved information. The SEM-EDX results are reported according to the salt type.

Microscopy observations on NaCl-contaminated specimens

Fig. 13 shows the EDX false-colour maps for specimens of AL, NHL and AC plaster contaminated with NaCl. For clarity reasons, only calcium (Ca, as a marker for the aggregate), silicon (Si, as a marker for the binder fraction), sodium and chlorine (Na, Cl, as markers for the salts) are shown. It is possible to observe that in all cases NaCl has accumulated in the outer millimetres of the plaster, up to 1,5–2,5 mm depth from the evaporation surface (see, for example, Fig. 13, white arrows in NHL plaster). Some isolated salt clusters can be observed in depth as well: these are fewer in AL plaster, and more numerous in NHL and even more in AC plaster (Fig. 13, black arrows in AC plaster). These slight differences in the salt distribution in depth are in agreement with the HMC results (Fig. 12) and can be explained by the different absorption and drying rates of the plasters (Figs. 4–5): the quicker absorption and drying of the AL plaster, due to the presence of coarse capillary pores (in the range 5–20 µm, Fig. 3), favours salt accumulation in a thin surface layer.

NaCl seems to start crystallizing preferentially at the binder/aggregate interface and on the pore walls of the larger pores, and to subsequently grow to fill empty spaces (Fig. 14, see, for example, black arrows in AC plaster). In the case of AL plaster, severe damage in the form of cracks and loss of cohesion is observed as a result of salt accumulation and crystallization at the binder/aggregate interface (Fig. 14, black arrows); the salt matrix seems to cement the loose particles together. Cracks are present in NHL and AC plasters too, but in a lower amount than in AL plaster. This difference might be related to the higher NaCl accumulation in a thinner layer of material observed in the AL plaster in comparison to the other plasters; this can result in a higher degree of pore filling and crystallization pressures [12] which likely overcomes the tensile strength of the plaster and leads to cracks. A more precise and quantitative assessment of the salt content and distribution (e.g. by ion chromatography analyses on samples collected with steps of 1 mm thickness as done in [44]) could support this hypothesis.

Microscopy observations on Na_2SO_4-contaminated specimens Fig. 15 shows the EDX maps of AL, NHL and AC plaster contaminated with Na_2SO_4. For clarity reasons, only calcium (Ca, as a marker for the aggregate), silicon (Si, as a marker for the binder fraction), sodium and sulphur (Na, S, as markers for the salts) are shown. Similarly to what observed in NaCl-contaminated specimens, also in this case salt has accumulated in the outer millimetres of the plaster; however, in this case the salt-enriched layer is thicker (up to 4,5 mm from the evaporation surface) than in NaCl specimens (Fig. 15, see, for example, white arrows in NHL plaster). Also in this case, the SEM-EDX observations confirm the HMC results, which showed salt accumulation in the outer 5 mm of the plaster layer. These results confirm the tendency of sodium chloride to be easily transported towards the evaporation surface, whereas sodium sulphate tends to crystallize right underneath it.

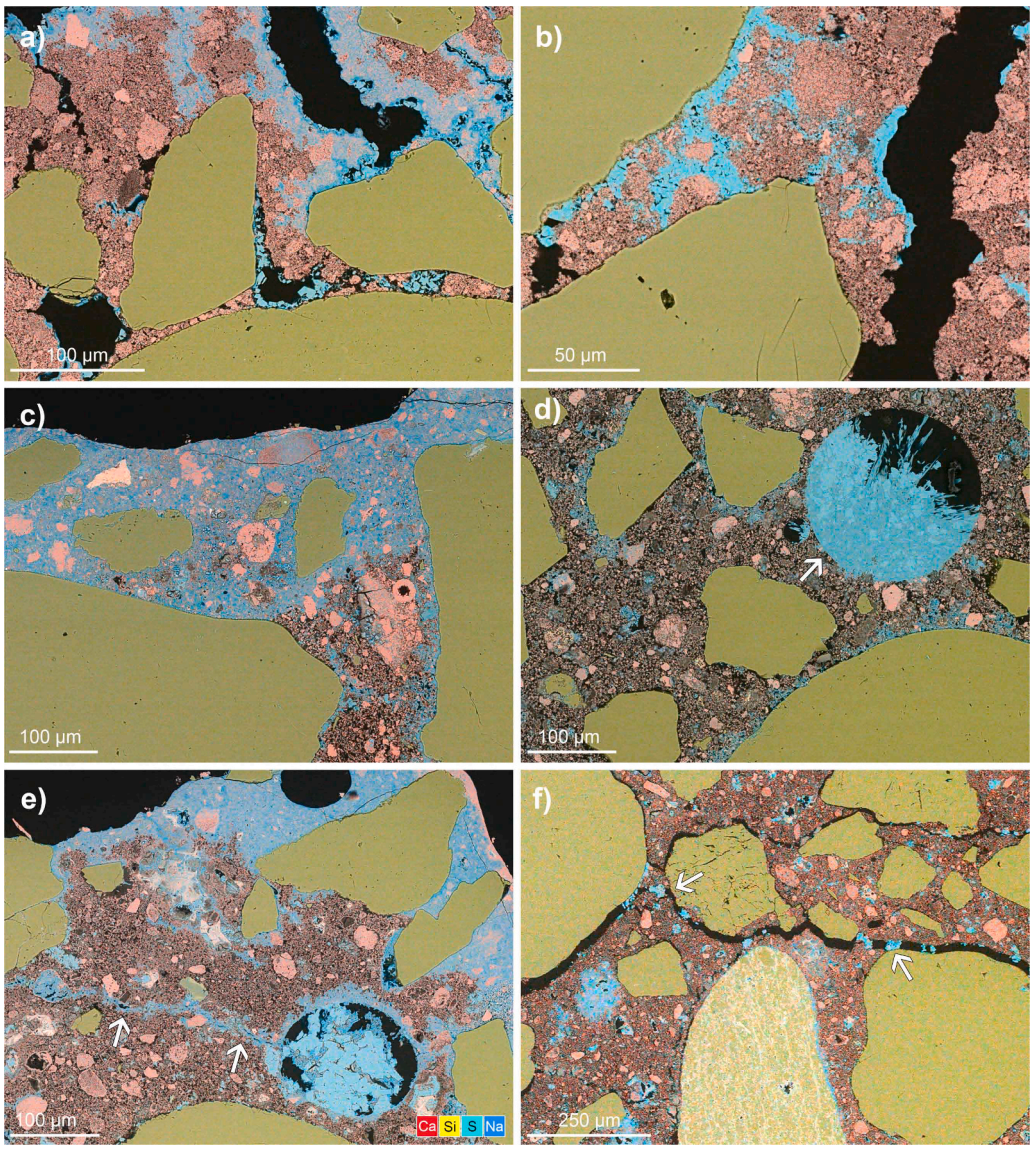

Fig. 16. EDX maps of the areas near the evaporation surface of AL (a,b), NHL (c,d) and AC (e,f) plaster specimens, contaminated with Na_2SO_4, at the end of the test.

Looking more closely at the location of salt crystallization, salts seem to fill small pores within the binder matrix, creating a compact, fine textured, salt-binder structure (Fig. 16a,b,c,e); some large, isolated crystals are observed sometimes in the cracks (Fig. 16f, arrows) and larger, needle-like cluster developed inside some of the round air bubbles present in NHL and AC plasters (Fig. 16d,e, arrow). This crystallization pattern is different from that of NaCl, which was observed to preferentially grow in cracks and/or along the pore walls. Very thin cracks, parallel to the evaporation surface, are present in all the plasters (Fig. 16e, arrows). These cracks suggest that the salt accumulation, and thus high degree of pore filling, in this area of the plaster has led to high crystallization pressures propagating through the pore network and overcoming the tensile strength of the plaster, consequently leading to cracks. However, no evident loss of material is observed in the areas affected by such cracks. This, together with the large amount of salt in the binder, suggests that the salt is cementing the loose particles of the plaster together.

4. Discussion and conclusions

In this research, a salt weathering procedure, based on the adaptation of the RILEM 271-ASC recommendation, has been applied on three plaster types, based on hydrated lime, natural hydraulic lime and hydrated lime-cement binders. Cylindrical specimens consisting of a porous stone substrate with 2 cm plaster layer applied on top, were contaminated with NaCl and Na_2SO_4 solutions and subjected to wet-dry cycles over about 4 months.

During the test salts were effectively transported from the substrate into the plaster layer, where they accumulated and caused damage due to repeated dissolution/crystallization cycles. Damage appeared as sanding and scaling, and its severity increased as the test propagation cycles progressed. NaCl-contaminated specimens showed moderate, comparable material across all plaster types, though AL plaster exhibited more severe cracking and cohesion loss than NHL and AC plasters. This may be attributed to the higher accumulation of NaCl—and consequently a greater degree of pore filling—within a thinner surface layer in the AL plaster, leading to more severe damage.

In the case of Na_2SO_4-contaminated specimens, visible material loss occurred only in the lime–cement plaster (AC), though all samples showed salt accumulation, cracks, and salt-filledvoids in the outer layer of the plaster, suggesting further cycles would likely lead to visible damage and material loss in AL and NHL plasters as well.

In general, material loss was larger in the case of NaCl contaminated specimens than in Na_2SO_4 contaminated ones, as observed also in other

experiments applying the RILEM TC 271-ASC procedure on stone and brick substrates [10]. This is possibly linked to the higher number of dissolution/crystallization cycles (induced by RH cycles) in the propagation phase compared to the Na_2SO_4 one. Additionally, the different salts might induce cementing effects on the plaster particles to different degrees at the end of the procedure.

The HMC measurements of the salt distribution in depth showed that salts accumulate in the outer layer (0–5 mm) of the plaster, independently of the type of salt and plaster. AL plasters showed a slightly higher salt accumulation in a thinner layer of the plaster, which can be explained by the presence of coarse capillary-active pores in this plaster, responsible for the observed faster absorption and drying behavior. Salt accumulation increased as the wet-dry cycles progressed. SEM observations, supported by EDX analyses, confirmed the HMC results, and allowed assessing salt distribution with higher resolution. The salt-rich layer formed close to the specimens' surface is thinner in NaCl contaminated plasters than in Na_2SO_4 ones; this confirms the higher tendency of NaCl to accumulate at the evaporation surface. Additionally, SEM-EDX observations highlighted differences in the crystallization pattern of the salts: while NaCl tends to crystallize in cracks, at the interface between aggregate and binder and at the surface of pores and voids, Na_2SO_4 is observed to crystallize preferentially in the small pores of the binder, or in the form of large, isolated crystals in cracks.

With respect to the proposed test weathering procedure, it can be concluded that, in general, the procedure proved to be effective, as it successfully induced damage within a period of 4 months. This is a much shorter time than needed by other procedures which consider combinations of materials, such as the RILEM MS-A.1 recommendation [23].

The type of damage observed in the plaster is representative of the damage observed in the field on these materials. The effectiveness of the test can possibly be improved by increasing the amount of salts in the specimens: to avoid the use of too high salt concentrations, the use of thicker stone substrate (e.g., 5 cm) can be considered. This would increase the volume of solution introduced during the contamination phase without affecting the salt solution concentration.

The monitoring methods and investigation techniques used for assessment of the damage and of the salt distribution have been proven suitable for the scope. In particular, SEM-EDX observations could precisely identify differences in crystallization patterns and microstructural damage in depth. Additionally, SEM-EDX allowed to visualize the cementing effect of the salts, which is preventing further material loss. This last observation suggests that, for a more realistic assessment of the decay, an extra step could be added to the test procedure, consisting of wetting the surface of the specimens to dissolve the salts and release the plaster particles no longer mechanically anchored to undamaged substrate.

These experiments constitute a first step in the validation of the proposed test procedure. Further assessment of the procedure on different plaster types, including plasters with mixed-in water repellent (salt accumulating plasters [28]), is desirable for a more thorough validation.

CRediT authorship contribution statement

Barbara Lubelli: Writing – original draft, Methodology, Investigation, Funding acquisition, Conceptualization. **Davide Gulotta:** Writing – review & editing, Investigation.

Declaration of Competing Interest

The authors declare the following financial interests/personal relationships which may be considered as potential competing interests: Barbara Lubelli reports financial support was provided by The Getty Conservation Institute. Barbara Lubelli reports a relationship with The Getty Conservation Institute that includes: funding grants and travel reimbursement. If there are other authors, they declare that they have no known competing financial interests or personal relationships that could have appeared to influence the work reported in this paper.

Acknowledgment

The authors wish to thank Ameya Kamat for performing the mechanical tests. This research has been supported by the Conservation Guest Scholar Program 2023-2024.

Data availability

Data will be made available on request.

References

[1] A.E. Charola, C. Bläuer, Salts in Masonry: An Overview of the Problem, Restor. Build. Monum. 21 (2015) 119–135, https://doi.org/10.1515/rbm-2015-1005.
[2] E. Doehne, Salt weathering: a selective review, Geol. Soc. Lond. Spec. Publ. 205 (2002) 51–64, https://doi.org/10.1144/GSL.SP.2002.205.01.05.
[3] A. Goudie, H. Viles, Salt weathering hazards, Wiley & Sons, 1997.
[4] G. Castellazzi, C. Colla, S. De Miranda, G. Formica, E. Gabrielli, L. Molari, F. Ubertini, A coupled multiphase model for hygrothermal analysis of masonry structures and prediction of stress induced by salt crystallization, Constr. Build. Mater. 41 (2013) 717–731, https://doi.org/10.1016/j.conbuildmat.2012.12.045.
[5] L. Grementieri, F. Daghia, L. Molari, G. Castellazzi, H. Derluyn, V. Cnudde, S. de Miranda, A multi-scale approach for the analysis of the mechanical effects of salt crystallisation in porous media, Int. J. Solids Struct. 126–127 (2017) 225–239, https://doi.org/10.1016/j.ijsolstr.2017.08.009.
[6] B. Lubelli, V. Cnudde, T. Diaz-Goncalves, E. Franzoni, R.P.J. van Hees, I. Ioannou, B. Menendez, C. Nunes, H. Siedel, M. Stefanidou, V. Verges-Belmin, H. Viles, Towards a more effective and reliable salt crystallization test for porous building materials: state of the art, Mater. Struct. /Mater. Constr. 51 (2018), https://doi.org/10.1617/s11527-018-1180-5.
[7] R.J. Flatt, N.A. Mohamed, F. Caruso, H. Derluyn, J. Desarnaud, B. Lubelli, R. M. Espinosa-Marzal, L. Pel, C. Rodriguez-Navarro, G.W. Scherer, N. Shahidzadeh, M. Steiger, Predicting salt damage in practice: a theoretical insight into laboratory tests, RILEM Tech. Lett. 2 (2017) 108–118, https://doi.org/10.21809/rilemtechlett.2017.41.
[8] B. Lubelli, R.P.J. van Hees, T.G. Nijland, Salt crystallization damage: how realistic are existing ageing tests? in: H. de Clerq (Ed.), Proceedings of the 3rd International Conference on Salt Weathering of Buildings and Stone Sculptures Royal Institute for Cultural Heritage, 2014, pp. 259–273.
[9] B. Lubelli, I. Rörig-Daalgard, A.M. Aguilar, M. Aškrabić, K. Beck, C. Bläuer, V. Cnudde, A.M. D'Altri, H. Derluyn, J. Desarnaud, T. Diaz Gonçalves, R. Flatt, E. Franzoni, S. Godts, D. Gulotta, R. van Hees, I. Ioannou, A. Kamat, T. De Kock, B. Menendez, S. de Miranda, C. Nunes, E. Sassoni, N. Shahidzadeh, H. Siedel, Z. Slížková, M. Stefanidou, M. Theodoridou, R. Veiga, V. Vergès-Belmin, Recommendation of RILEM TC 271-ASC: New accelerated test procedure for the assessment of resistance of natural stone and fired-clay brick units against salt crystallization, Mater. Struct. /Mater. Constr. 56 (2023), https://doi.org/10.1617/s11527-023-02158-0.
[10] B. Lubelli, A.M. Aguilar, K. Beck, T. de Kock, J. Desarnaud, E. Franzoni, D. Gulotta, I. Ioannou, A. Kamat, B. Menendez, I. Rorig-Dalgaard, E. Sassoni, A new accelerated salt weathering test by RILEM TC 271-ASC: preliminary round robin validation, Mater. Struct. / Matér. Constr. 55 (2022) 238, https://doi.org/10.1617/s11527-022-02067-8.
[11] K. Tuutti, Corrosion of steel in concrete, Stockholm, 1982.
[12] R.J. Flatt, F. Caruso, A.M.A. Sanchez, G.W. Scherer, Chemo-mechanics of salt damage in stone, Nat. Commun. 5 (2014) 4823, https://doi.org/10.1038/ncomms5823.
[13] H.J.P. Brocken, Moisture transport in brick masonry: the grey area between bricks (PhD thesis), Technische Universiteit Eindhoven, 1998, https://doi.org/10.6100/IR519159.
[14] J. Petković, H.P. Huinink, L. Pel, K. Kopinga, R.P.J. Van Hees, Salt transport in plaster/substrate layers, Mater. Struct. /Mater. Constr. 40 (2007) 475–490, https://doi.org/10.1617/s11527-006-9151-7.
[15] C. Nunes, L. Pel, J. Kunecký, Z. Slížková, The influence of the pore structure on the moisture transport in lime plaster-brick systems as studied by NMR, Constr. Build. Mater. 142 (2017) 395–409, https://doi.org/10.1016/j.conbuildmat.2017.03.086.
[16] WTA Sanierputzsysteme Merkblatt 2–9-04D.pdf, (2004)
[17] T. Wijffels, B. Lubelli, Development of a new accelerated salt crystallization test, Heron 51 (2006) 63–75.
[18] A. Kamat, E. Schlangen, B. Lubelli, Encapsulated crystallisation inhibitor as a long-term solution to mitigate salt damage in hydraulic mortars, Cem. Concr. Compos 152 (2024) 105682, https://doi.org/10.1016/j.cemconcomp.2024.105682.
[19] S.J.C. Granneman, B. Lubelli, R.P.J. Van Hees, Effect of mixed in crystallization modifiers on the resistance of lime mortar against NaCl and Na2SO4 crystallization, Constr. Build. Mater. 194 (2019) 62–70, https://doi.org/10.1016/j.conbuildmat.2018.11.006.
[20] CEN, EN 196-1 - Methods of testing cement - Part 1: Determination of strength, (2005).

[21] CEN, EN 1015-3 - Methods of test for mortar for masonry - Part 3: Determination of consistence of fresh mortar (by flow table), (1999).
[22] B. Lubelli, R.P.J. van Hees, T.G. Nijland, J. Bolhuis, A new method for making artificially weathered stone specimens for testing of conservation treatments, J. Cult. Herit. 16 (2015) 698–704, https://doi.org/10.1016/j.culher.2015.01.002.
[23] RILEM TC 127-MS, MS-A.1 Determination of the resistance of wallettes against sulphates and chlorides, Mater. Struct. 31 (1998) 2–9, https://doi.org/10.1007/bf02486406.
[24] C.J.W.P. Groot, Effect of mortar on water brick bond (PhD thesis), TU Delft, 1993.
[25] T. Wijffels, R. van Hees, The influence of the loss of water of the fresh mortar to the substrate on the hygric characteristics of so-called restoration plaster, in: Proceeding of the Int. Workshop on Urban Heritage and Building Maintenance VII, 2000: pp. 49–54.
[26] CEN, EN 1015-11 - Methods of test for mortar for masonry - Part 11: Determination of flexural and compressive strength of hardened mortar, (1999).
[27] L.J.A.R. van der Klugt, J.A.G. Koek, De kwaliteit van voegen in metselwerk, SBR, 1994.
[28] C. Groot, R. van Hees, T. Wijffels, Selection of plasters and renders for salt laden masonry substrates, Constr. Build. Mater. 23 (2009) 1743–1750, https://doi.org/10.1016/j.conbuildmat.2008.09.013.
[29] T. Wijffels, B. Lubelli, Development of a new accelerated salt crystallization test, Heron 51 (2006) 63–75.
[30] C. Rodriguez-Navarro, E. Doehne, E. Sebastian, How does sodium sulfate crystallize? Implications for the decay and testing of building materials, Cem. Concr. Res. 30 (2000) 1527–1534, https://doi.org/10.1016/S0008-8846(00)00381-1.
[31] J. Desarnaud, F. Bertrand, N. Shahidzadeh-Bonn, Impact of the kinetics of salt crystallization on stone damage during rewetting/drying and humidity cycling, J. Appl. Mech. 80 (2013) 020911, https://doi.org/10.1115/1.4007924.
[32] J. Desarnaud, N. Shahidzadeh-Bonn, Salt crystal purification by deliquescence/crystallization cycling, Epl 95 (2011), https://doi.org/10.1209/0295-5075/95/48002.
[33] B. Lubelli, R.P.J. van Hees, Irreversible dilation of NaCl contaminated lime-cement mortar due to crystallization cycles, Cem. Concr. Res. 36 (2006) 678–687.
[34] B. Lubelli, A.M. Aguilar, K. Beck, T. de Kock, J. Desarnaud, E. Franzoni, D. Gulotta, I. Ioannou, A. Kamat, B. Menendez, I. Rorig-Dalgaard, E. Sassoni, A new accelerated salt weathering test by RILEM TC 271-ASC: preliminary round robin validation, Mater. Struct. 55 (2022) 238, https://doi.org/10.1617/s11527-022-02067-8.
[35] B. Lubelli, V. Cnudde, T. Diaz-Goncalves, E. Franzoni, R.P.J. van Hees, I. Ioannou, B. Menendez, C. Nunes, H. Siedel, M. Stefanidou, V. Verges-Belmin, H. Viles, Towards a more effective and reliable salt crystallization test for porous building materials: state of the art, Mater. Struct. /Mater. Constr. 51 (2018), https://doi.org/10.1617/s11527-018-1180-5.
[36] B. Lubelli, R.P.J. Van Hees, H.J.P. Brocken, Experimental research on hygroscopic behaviour of porous specimens contaminated with salts, Constr. Build. Mater. 18 (2004) 339–348, https://doi.org/10.1016/j.conbuildmat.2004.02.007.
[37] T. Diaz Gonçalves, J. Delgado Rodrigues, Evaluating the salt content of salt-contaminated samples on the basis of their hygroscopic behavior. Part I: fundamentals, scope and accuracy of the method, J. Cult. Herit. 7 (2006) 79–84, https://doi.org/10.1016/j.culher.2006.02.009.
[38] T.D. Gonçalves, J.D. Rodrigues, M.M. Abreu, Evaluating the salt content of salt-contaminated samples on the basis of their hygroscopic behaviour: Part II: experiments with nine common soluble salts, J. Cult. Herit. 7 (2006) 193–200, https://doi.org/10.1016/j.culher.2006.03.002.
[39] M. Nasraoui, W. Nowik, B. Lubelli, A comparative study of hygroscopic moisture content, electrical conductivity and ion chromatography for salt assessment in plasters of historical buildings, Constr. Build. Mater. 23 (2009) 1731–1735, https://doi.org/10.1016/j.conbuildmat.2008.09.029.
[40] C. Gentilini, E. Franzoni, S. Bandini, L. Nobile, Effect of salt crystallisation on the shear behaviour of masonry walls: an experimental study, Constr. Build. Mater. 37 (2012) 181–189, https://doi.org/10.1016/j.conbuildmat.2012.07.086.
[41] C. Rodriguez-Navarro, E. Doehne, Salt weathering: influence of evaporation rate, supersaturation and crystallization pattern, Earth Surf. Process Land. 24 (1999) 191–209, https://doi.org/10.1002/(SICI)1096-9837(199903)24:3<191::AID-ESP942>3.0.CO;2-G.
[42] T.C.D. Gonçalves, Salt crystallization in plastered or rendered walls, PhD, Universidade Tecnica de Lisboa, 2007.
[43] B. Lubelli, R.P.J. Van Hees, H.J.P. Brocken, Experimental research on hygroscopic behaviour of porous specimens contaminated with salts, Constr. Build. Mater. 18 (2004) 339–348, https://doi.org/10.1016/j.conbuildmat.2004.02.007.
[44] D. Gulotta, Comparative estimation of the pore filling of single salts in natural stone, in: B. Lubelli, A. Kamat, W. Quist (Eds.), Fifth International Conference on Salt Weathering of Buildings and Stone Sculptures, TU Delft Open, 2021.